Resonance-enhanced Coupling for Range Extension of Electromagnetic Tracking Systems

Mohd Noor Islam[1], Andrew J. Fleming[2]
School of Electrical Engineering and Computer Science
The University of Newcastle
Callaghan, Australia

This article investigates the use of resonance-enhanced coupling to increase the received signal level in a six degree-of-freedom electromagnetic tracking system. Resonant coupling is found to increase the efficiency of the transmitter and increase the gain of the sensing coil, resulting in improved range. However, the measurement update rate is reduced due to the settling-time of the transmitter circuit and limited bandwidth of the sensing circuit. A resistive tuning approach is proposed to balance the trade-off between a decreased measurement bandwidth and improved signal level.

***Index Terms*—Capsule endoscopy, Tracking system, Resonance, Measurement range, Bandwidth.**

I. Introduction

Electromagnetic (EM) tracking systems are used extensively in biomedical devices, gaming consoles, and animation because they are inexpensive and do not require line of sight. Electromagnetic tracking systems for catheters and endoscope capsules have shown promising results [1]–[10]. However, at present, commercial capsules take 6-8 hours for a whole gastrointestinal (GI) tract endoscopy due to the natural peristalsis movement [11]. Some parts of the GI tract remain unobserved due to limited battery life. Magnetic maneuvering can speed the capsule's movement and result in a faster diagnosis [12], [13].

Two of the foremost challenges in EM tracking systems are increasing both the measurement range and rate, which are contradictory due to the relationship between the noise variance and bandwidth. The measurement range is limited by the amplitude of the induced voltage in the sensing coil, which is determined by the transmitted power and coil construction [14], [15]. The induced voltage can also be amplified but this does not improve the underlying signal-to-noise ratio [16].

This article investigates the use of resonance-enhanced coupling to extend the range and improve the signal-to-noise ratio in a selected frequency band. Resonance enhanced coupling is ubiquitous in wireless power transmission systems due to the high efficiency [17]–[20]. In this article, these methods are applied to increase the induced voltage in an electromagnetic localization system [21]. Resonance in the transmitting coil improves the energy efficiency and resonance in the sensing coil passively increases the signal gain.

Although a resonant circuit significantly improves the signal gain, the settling-time of the system is also increased, which is detrimental to the measurement bandwidth. Sequential commutation of a resonant array of transmitting coils with a single capacitor can avoid the transient [22] if the coil inductances are well matched. By considering the settling-time of both the transmitter and receiver, this article describes the use of resistive tuning to control the trade-off between the measurement bandwidth and signal gain.

A six-degree-of-freedom EM tracking systems is composed of three concentric, orthogonal transmitting and sensing coils [23]–[34]. A six-degree-of-freedom EM capsule tracking system is shown in Fig. 1. Commercial EM tracking systems can be grouped into two categories: those with sequential excitation of the coils, such as the Hydra system [23], [35], or where the transmitting coils are excited simultaneously [35]. Although simultaneous excitation is faster, due to the parallel measurements, multiple frequencies are required in addition to a more complex demodulation scheme. In simultaneous excitation, the settling-time of the transmitter becomes irrelevant.

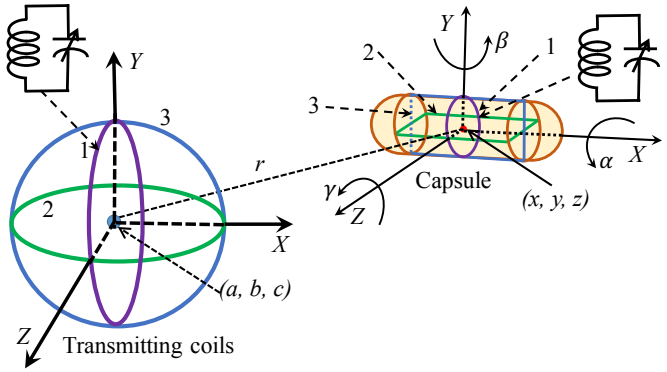

Fig. 1: Six-degree-of-freedom electromagnetic capsule tracking system. Sensing coils in the capsule are shown in violet, blue and green.

Expressions for the settling-time, efficiency, and signal gain are derived analytically and are experimentally verified on an endoscope capsule system described in [21]. The resistive tuning method is demonstrated to provide control over the trade-off between the measurement bandwidth and the signal gain.

In the following section, the transmitting and sensing coil parameters are described. Sections III, IV and V describe the transmitter, compare the different methods for transmitter coil enhancement, and analyze the tuning method. Likewise, Sections VI, VII and VIII describe the sensing system, compare the methods for sensing coil enhancement, and analyze the

TABLE I: Parameters of the EM tracking system.

R_T	Resistance of the transmitting coil.
L_T	Inductance of the transmitting coil.
C_T	Self-capacitance of the transmitting coil.
R_s	Resistance of the sensing coil.
L_s	Inductance of the sensing coil.
C_s	Self-capacitance of the sensing coil.
I_T	Amplitude of the transmitter source current.
I_L	Amplitude of the coil current.
A_i	Amplitude of the induced voltage.
A_s	Amplitude of the voltage of the sensing circuit.
τ	Time constant.
r	Sensing range.
t_T	Settling time of the transmitter.
t_s	Settling time of the sensing circuit.
Q	Quality factor of the sensing circuit
G	Gain of the sensing circuit.
$\chi_{s,ser}$	Settling time variation factor. The ratio of setting times with and without inclusion of an external series resistor.
$\chi_{s,par}$	Settling time variation factor. The ratio of setting times with and without the inclusion of an external parallel resistor.
K	Ratio of external resistance and coil resistance.

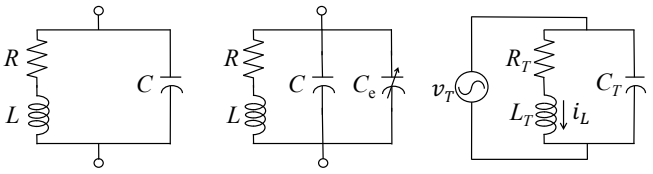

(a) Eqv. coil circuit (b) Identify parameters (c) Transmitter

Fig. 2: (a) Equivalent circuit of a coil. (b) Circuit for measuring coil parameters. (c) Transmitter circuit.

tuning method. The results are summarized in Section V for the transmitter and in Section VIII for the sensing system. The measurement bandwidth and rate are explained in Section IX . The experimental results on measurement noise is summarized in Section X. The article is concluded in XI.

II. Coil Parameter Identification

At high frequencies, the response of a coil can be described by the self-capacitance in parallel with resistance and inductance, as shown in Fig. 2 (a). The coil parameters R, L and C can be determined by using an LCR meter and an additional capacitance C_e, as shown in Fig. 2 (b). By varying C_e, and measuring the impedance, the parameters can be identified. If two values of C_e are C_{e1} and C_{e2}, and the corresponding resonance frequencies are f_1 and f_2, the relationship between the resonance frequencies and the coil capacitance is

$$C = \frac{\left(\frac{f_2}{f_1}\right)^2 C_{e2} - C_{e1}}{1 - \left(\frac{f_2}{f_1}\right)^2}. \tag{1}$$

The coil's self-inductance L can be calculated from either

$$L = \frac{1}{4\pi^2 f_1^2 \left(C + C_{e1}\right)}, \tag{2}$$

TABLE II: Typical parameters of the transmitting and sensing coil in an electromagnetic endoscope capsule tracking system.

Transmitting coil	R_T	L_T	C_T
	1.3 Ω	472 µH	109 pF
Sensing coil	R_s	L_s	C_s
	20.4 Ω	287 µH	49 pF

or

$$L = \frac{1}{4\pi^2 f_2^2 \left(C + C_{e2}\right)}. \tag{3}$$

The resistance R at f_1 is

$$R = \frac{2\pi f_1^2 L^2}{Z_1}. \tag{4}$$

However, due the the skin-effect, the resistance R' at another frequency $f < f_1$ is [36]

$$R' = R\left(1 - \left(\frac{f}{f_1}\right)^2\right). \tag{5}$$

Since the desired operating frequency is typically close to the frequency used for parameter identification, the frequency dependence of the resistance can often be neglected.

The identified coil parameters of the experimental six-degree-of-freedom endoscope system shown in Fig. 1 are listed in Table II [21].

III. Transmitter Analysis

The equivalent transmitter circuit is shown in Fig. 2 (c). The applied voltage to the transmitter is $v_T(t) = A_T \sin(\omega t)$. The equation for the current through the transmitting coil can be written as

$$L_T \frac{di_L}{dt} + R_T i_L = A_T \sin(\omega t). \tag{6}$$

The solution of (6) is

$$i_L(t) = \frac{R_T A_T}{D} \sin\omega t - \frac{\omega L_T A_T}{D} \cos\omega t + \frac{\omega L_T A_T}{D} e^{\frac{-R_T t}{L_T}}, \tag{7}$$

where $D = R_T^2 + (\omega L_T)^2$. The coil current reaches steady state after the transient component decays. The time constant of the transmitter circuit is

$$\tau_T = -\frac{L_T}{R_T} \ln(0.368). \tag{8}$$

The magnitude of the transient component is below 3% of its maximum value after four time constants, so the settling-time of the transmitting circuit is

$$t_T = 4\tau_T = -4\frac{L_T}{R_T} \ln(0.368). \tag{9}$$

The settling-time is proportional to L_T and inversely proportional to R_T. Therefore, the settling-time of the transmitter depends on its construction parameters, such as length, radius, number of turns, diameter of the wire, and the core. For electromagnetic tracking systems, the transmitting coil parameters need to be optimized to maximize the resulting field strength [37].

IV. Transmitter Resonance Enhancement

EM tracking systems for portable applications such as endoscopy, catheter tracking, and virtual reality require a lightweight and energy efficient transmitter. Resonance in the transmitting coil can improve the efficiency at the expense of settling-time. The two circuit options, series and parallel resonance, are examined in the following.

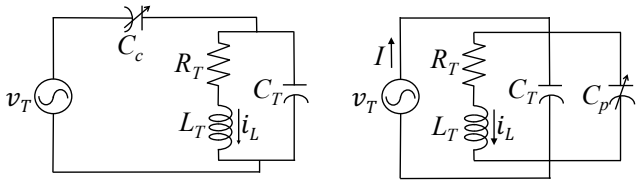

(a) Series resonance (b) Parallel resonance

Fig. 3: Equivalent transmitter circuits with series and parallel resonance.

A. Series Transmitter Resonance

The current through the transmitting coil in the series resonant circuit shown in Fig. 3 (a) is

$$L_T C_q \frac{d^2 i_L}{dt^2} + R_T C_q \frac{di_L}{dt} + i_L = C_c A_T \omega \cos \omega t, \qquad (10)$$

where $(C_T + C_c) = C_q$. By solving (10), the time constant of the series resonant transmitter circuit is

$$\tau_{T,ser} = -\frac{2L_T}{R_T} \ln (0.368) . \qquad (11)$$

By comparing (8) and (11), it is clear that the settling-time of the transmitter circuit is doubled in series resonance. The coil current amplitude amplification factor is $\sqrt{(R_T^2 + (\omega_0 L_T)^2)}/R_T$, where $\omega_0 = 2\pi f_0$ and $C_c \gg C_T$. The amplitude of the coil current in the series configuration is

$$I_{L,ser} = \frac{A_T}{R_T} \qquad (12)$$

which is equal to the transmitter source current.

B. Parallel Transmitter Resonance

The transmitter coil current in the parallel resonant circuit shown in Fig. 3 (b) is

$$L_T \frac{di_L}{dt} + R_T i_L = A_T \sin (\omega t) . \qquad (13)$$

By solving (13), the time constant of the transmitter circuit due to parallel resonance is

$$\tau_{T,par} = -\frac{L_T}{R_T} \ln (0.368) . \qquad (14)$$

A comparison between (8) and (14) shows that parallel resonance does not increase the settling-time of the transmitter circuit. However, in the parallel configuration, the transmitter coil current is dependent on the resonance frequency, similar to the case without resonance. The amplitude of the coil current at resonance frequency f_0 is

$$I_{L,par} = \frac{A_T}{\sqrt{(R_T^2 + (\omega_0 L_T)^2)}}. \qquad (15)$$

The transmitter source current is $\omega_0 R_T C_T$ times the coil current, where $\omega_0 R_T C_T < 1$.

The choice of resonance circuit will depend on the available transmitter source voltage and current. For the same coil current, the required source voltage, source current, and resulting settling-time is listed in Table III. Example values for these quantities are listed in Table IV. The series configuration results in a low source voltage, while the parallel configuration results in a low source current and half the settling-time.

TABLE III: Source requirements and settling-time of series and parallel resonant transmitter circuits for a specified coil current $I_L = I_{L,ser} = I_{L,par}$ at resonance frequency f_0.

Resonance	Source voltage, A_T	Source current, I_T	Settling time
Series	$I_L R_T$	I_L	$-\frac{8L_T}{R_T} \ln (0.368)$
Parallel	$I_L \left(R_T^2 + (\omega_0 L_T)^2\right)^{1/2}$	$\omega_0 R_T C_q I_L$	$-\frac{4L_T}{R_T} \ln (0.368)$

TABLE IV: An example of the source voltage, source current, and settling-time for a series and parallel resonant transmitter circuit. Two cases are considered, one where the desired coil current is 1 A at 8 kHz, and another where the desired current is 1 A at 110 kHz. These cases are typical for the capsule tracking system described in Table II.

Resonance	Frequency (kHz)	Source voltage (V)	Source current (A)	Source power (V A)	Settling time (ms)
Series	8 or 110	1.3	1	1.3	2.9
Parallel	8	23.76	0.055	1.3	1.45
	110	326	0.004	1.3	1.45

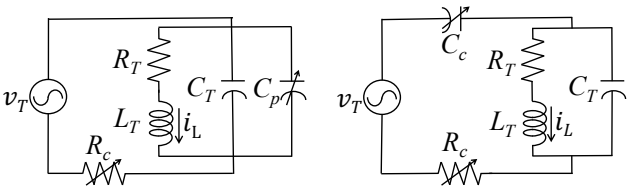

(a) Parallel resonance (b) Series resonance

Fig. 4: Equivalent parallel and series resonant transmitter circuits with external series resistance.

V. Resonant Transmitter Tuning

The implementation of resonance in the transmitter circuit results in increased settling-time, and consequently, increased measurement delay. In the following, a resistive tuning method is described which allows the trade-off between efficiency and settling-time to be freely manipulated.

A. Resistive Tuning in Series Resonance

By introducing an external series resistance, the settling-time of the series resonant transmitter circuit can be tuned. The

TABLE V: Summary of the transmitter source voltage and source current required to obtain a coil current of I_L with a settling-time of $t_T = t_{T,ser} = t_{T,par}$ at resonance frequency f_0.

Resonance	Source voltage, A_T	Source current, I_T	R_c
Series	$I_L\left(R_T + R_c\right)$	I_L	$-\frac{8L_T}{t_T}\ln\left(0.368\right) - R_T$
Parallel	$I_L\left(\left(R_T^2 + \left(\omega_0 L_T + \omega_0 R_T R_c C_q\right)^2\right)\right)^{1/2}$	$\omega_0 R_T C_q I_L$	$\frac{1}{2}\left(-\frac{4L_T}{t_T}\ln\left(0.368\right) - R_T\right)$

TABLE VI: Example transmitter source voltage and current required to achieve 1 A coil current and 100 µs settling-time. The resonance frequencies are 8 kHz and 110 kHz, which are typical for the capsule tracking system described in Table II.

Resonance	Frequency (kHz)	Source voltage (V)	Source current (A)	Source power (V A)	R_c (Ω)	Power loss in R_c
Series	8 or 110	37.74	1	37.74	36.45	36.45 W
Parallel	8	24.23	0.054	1.3	8.8	26.4 mW
	110	326	0.004	1.3	8.8	0.14 mW

equivalent circuit with additional resistance is shown in Fig. 4 (a). The additional resistance is a multiple of the coil resistance, i.e., $R_c = K_t \times R_T$.

With the additional resistance R_c, the coil current is described by

$$L_T C_c \frac{d^2 i_L}{dt^2} + \left(R_T + R_c\right) C_c \frac{di_L}{dt} + i_L = C_c A_T \omega \cos \omega t. \quad (16)$$

The settling-time is the solution of (16), which is

$$t_{T,ser} = -\left(\frac{8L_T}{\left(R_T + R_c\right)}\right)\ln\left(0.368\right). \quad (17)$$

The amplitude of the transmitter coil current is also modified to $A_T/(R_T + R_c)$.

B. Resistive Tuning in Parallel Resonance

The equivalent circuit of the parallel resonant transmitter with additional series resistance is shown in Fig. 4 (b). With an additional series resistance $R_c = K_t \times R_T$, the coil current is

$$L_T \frac{di_L}{dt} + \left(R_T + 2R_c\right) i_L = A_T \sin \omega t. \quad (18)$$

By solving (18), the time constant is

$$t_{T,par} = -\left(\frac{4L_T}{R_T + 2R_c}\right)\ln\left(0.368\right). \quad (19)$$

The amplitude of the coil current is the parallel resonant circuit is $A_T/\sqrt{\left(R_T^2 + \left(\omega_0 L_T + \omega_0 R_T R_c C_q\right)^2\right)}$. The coil current is insensitive to R_c when $\omega_0 L_T \gg \omega_0 R_T R_c C_q$; however, the settling-time reduces significantly in this range.

Table V summarizes the required source voltage and current required to achieve a certain coil current and settling-time. Example values for the endoscope tracking system are also listed in Table VI. Note that the series configuration requires a large additional resistor which significantly increases the required source power. On the other hand, the parallel configuration requires impractically high voltage at 110 kHz. To reduce settling-time, the parallel configuration is preferable so long as the required voltage is within practical limits.

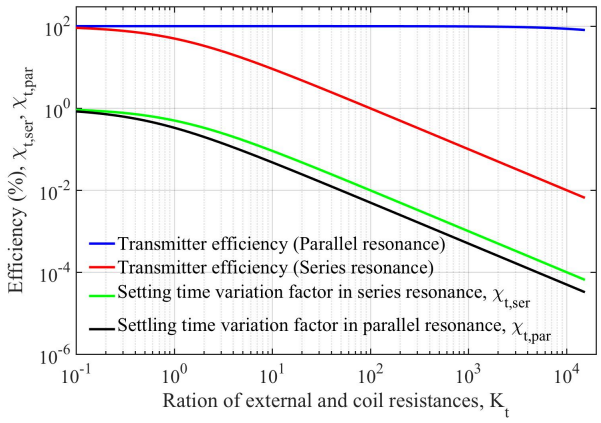

Fig. 5: The effect of external series resistance R_c on the efficiency and settling-time of the transmitter in series and parallel resonance, where $K_t = R_c/R_T$.

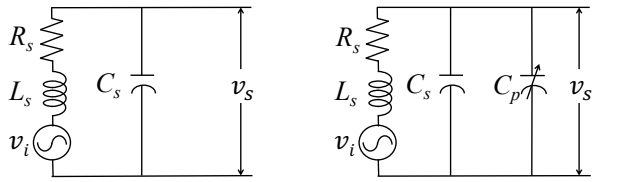

(a) Eqv. sensing coil circuit (b) With resonance tuning

Fig. 6: The sensing coil equivalent circuits.

In the series resonance configuration, the current through R_c reduces the source efficiency, whereas, in the parallel resonance, the power dissipation in R_c is negligible. Fig. 5 shows the trade-off between the settling-time and source efficiency, where $\chi_{t,ser}$ and $\chi_{t,par}$ are the ratios of the settling-times with and without R_c. The efficiency is the ratio of the power dissipated by the coil resistance R_T, to the power dissipated by both resistors R_T and R_c, expressed as a percentage.

VI. Sensing Coil Analysis

The received field by the sensing coil is proportional to $1/r^3$, where r is the distance between the transmitter and sensor. Therefore, if the sensor gain can be increased by a factor G, the extended range is $r_1 = rG^{1/3}$, i.e. the range is increased by $r\left(G^{1/3} - 1\right)$.

The equivalent circuit of a sensing coil is shown in Fig. 6(a). Let the induced voltage be $v_i(t) = A_i \sin\left(\omega t + \phi_1\right)$ and the output voltage across the coil capacitance C_s will be $v_s(t) = A_s \sin\left(\omega t + \phi_2\right)$. The differential equation of the output voltage v_s is

$$L_s C_s \frac{d^2 v_s}{dt^2} + R_s C_s \frac{dv_s}{dt} + v_s = v_i\left(t\right). \quad (20)$$

Since the internal capacitance of the sensing coil C_s is very low (49 pF), self-resonance occurs beyond 1 MHz. Therefore, the gain from v_i to v_s at frequencies in the kHz range is approximately unity.

A. Sensing Circuit Settling Time

The settling-time of the sensing circuit is

$$t_s = 4 \times \frac{2L_s}{R_s} \ln(0.368). \tag{21}$$

The quality factor of the sensing circuit Q_0 depends on the construction of the coil and the resonance frequency,

$$Q_0 = \frac{\omega_o L_s}{R_s} \tag{22}$$

VII. Sensing Coil Resonance Enhancement

The range of the tracking system can be increased either by strengthening the magnetic field [37], or by increasing the gain of the sensing circuit. A parallel resonant circuit passively amplifies the induced voltage. This reduces the effect of preamplifier noise and attenuates off-frequency environmental noise. The equivalent circuit diagram is shown in Fig. 6 (b) where C_p is the external capacitor. The differential equation for the output voltage v_0 across the capacitor C_p is

$$L_s C_q \frac{d^2 v_s}{dt^2} + R_s C_q \frac{dv_s}{dt} + v_s = v_i(t). \tag{23}$$

where $C_q = C_s + C_p$. To achieve a resonance frequency of f_0 Hz, the required capacitance is:

$$C_q = \frac{1}{4\pi^2 f_0^2 L_s} \tag{24}$$

A. Resonant Sensing Circuit Gain

The gain of the sensing circuit in Fig. 6 (b) is

$$|G_1(\omega)| = \frac{1}{\sqrt{(1-\omega^2 L_s C_q)^2 + (\omega R_s C_q)^2}}. \tag{25}$$

At resonance, the gain and quality factor Q_1 are

$$\left|\frac{A_s}{A_i}\right| = Q_1 = \frac{1}{\omega_0 R_s C_q}. \tag{26}$$

Example frequency responses for a range of external capacitances are plotted in Fig. 7. The bandwidth Δf of the circuit is independent of the capacitance, and is determined by

$$\Delta f = \frac{1}{2\pi}\frac{R_s}{L_s}. \tag{27}$$

B. Resonant Sensing Circuit Settling Time

The output voltage of the resonant sensing circuit can be determined by solving (23), which is

$$v_s(t) = \underbrace{K_1 \sin(\omega t) + K_2 \cos(\omega t)}_{\text{Steady-state output}} + \underbrace{K_3 e^{m_1 t} + K_4 e^{m_2 t}}_{\text{Transient output}}, \tag{28}$$

where

$$m = -\frac{R_s}{2L_s} \pm \sqrt{\left(\frac{R_s}{2L_s}\right)^2 - \frac{1}{L_s C_q}}. \tag{29}$$

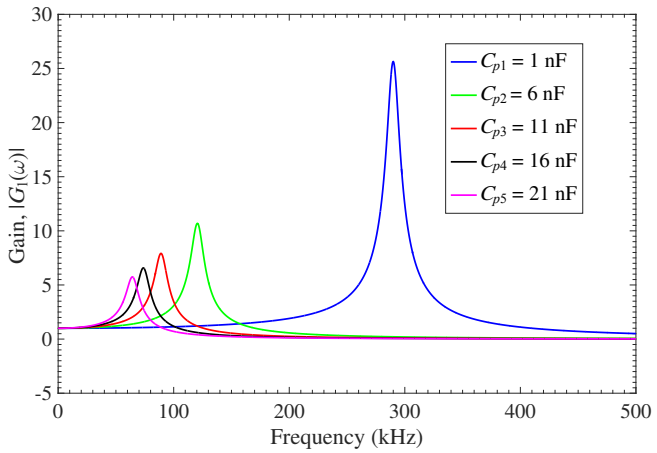

Fig. 7: Frequency responses of the sensing circuit for a range of parallel capacitances.

TABLE VII: Example sensor gain and settling-time of the prototype capsule system at resonance frequencies of 8 and 110 kHz. The coil parameters are listed in Table II.

f_0 (kHz)	C_q	Gain	Settling time (ms)
8	1.4 µF	0.7	0.112
110	7.3 nF	9.7	0.112

The time constant of the resonant sensing circuit is

$$\tau_{s,par} = -\frac{2L_s}{R_s} \ln(0.368) \tag{30}$$

That is, the settling-time is

$$t_{s,par} = -\frac{8L_s}{R_s} \ln(0.368). \tag{31}$$

The sensing coil has a low inductance but typically higher resistance than the transmitting coil. Therefore, the settling-time of the sensor can be significantly lower than the transmitter. Example values for the gain and settling-time are listed in Table II. The effect of resonance on the experimental system can be observed in Fig. 8.

VIII. Resonant Sensing Circuit Tuning

In order to control the trade-off between gain and settling-time in the sensor circuit, an external resistor can be added in parallel or series to the capacitor C_p as Fig. 9.

A. Resonant Sensing Circuit with Parallel Resistance

The equivalent circuit including the additional parallel resistance R_p, is shown in Fig. 9 (a). The equation for the output voltage is

$$L_s C_q \frac{d^2 v_s}{dt^2} + \left(R_s C_q + \frac{L_s}{R_p}\right)\frac{dv_s}{dt} + \left(\frac{R_s}{R_p} + 1\right) v_s = v_i(t). \tag{32}$$

At resonance, where $\omega = \omega_0$, the gain is

$$|G_2(\omega)|_{\omega=\omega_0} = \frac{1}{\sqrt{\left(\frac{R_s}{R_p}\right)^2 + \left(\omega_0\left(R_s C_q + \frac{L_s}{R_p}\right)\right)^2}}. \tag{33}$$

TABLE VIII: Summary of the required C_p and R_c or R_p to achieve a resonance frequency f_0 and settling-time t_s.

External resistance in	C_q	R_c or R_p	Gain
Parallel	$\frac{1}{4\pi^2 f_0^2 L_s}$	$-\left(\frac{t_s L_s}{t_s R_s C_q + 8 L_s C_q \ln(0.368)}\right)$	$\frac{1}{\left(\left(\frac{R_s}{R_p}\right)^2+\left(\omega_0\left(R_s C_q+\frac{L_s}{R_p}\right)\right)^2\right)^{1/2}}$
Series	$\frac{1}{4\pi^2 f_0^2 L_s}$	$-\frac{8L_s}{t_s}\ln(0.368) - R_s$	$\frac{\left(1+(\omega_0 R_c C_p)^2\right)^{1/2}}{\omega_0 C_q (R_s+R_c)}$

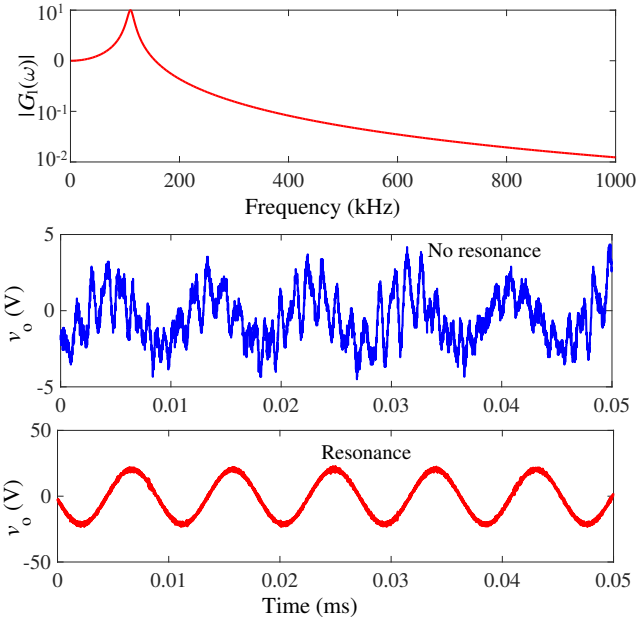

Fig. 8: The frequency response and measured output voltage of the experimental localization system with a 110 kHz resonance frequency.

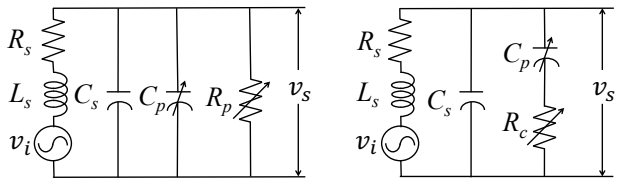

(a) Parallel resistor (b) Series resistor

Fig. 9: Tuning the sensing circuit with an external resistor in parallel or series with the external capacitor.

The variation in settling-time due to the additional parallel resistance can be described by the settling-time variation factor $\chi_{s,par}$, which is the ratio of the settling-time with and without the parallel resistance. That is, the settling-time variation factor of the sensing circuit is

$$\chi_{s,par} = \frac{1}{1+\frac{L_s}{R_s^2(R_p/R_s)C_q}}. \tag{34}$$

The quality factor of the resonant sensing circuit will also be affected due to the additional parallel resistance. By neglecting C_s, the quality factor is

$$Q_2 = \frac{\omega_o L_s\left(\frac{L_s}{R_1^2}+C_q\right)}{\frac{L_s}{R_p}+\frac{R_s L_s}{R_p^2}+R_s C_q}. \tag{35}$$

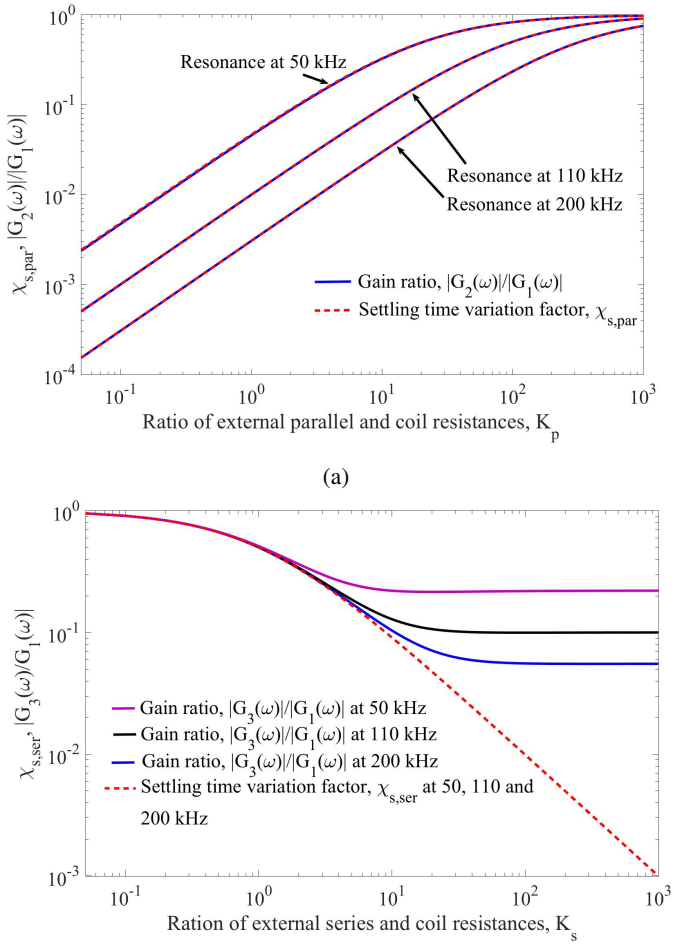

Fig. 10: The gain ratio and settling-time versus (a) the parallel resistance, where $K_p = R_p/R_s$, and (b) the series resistance, where $K_s = R_c/R_s$.

B. Resonant Sensing Circuit with Series Resistance

The circuit with additional series resistance R_c is shown in Fig. 9. By ignoring C_s, the voltage across the capacitor C_p is

$$L_s C_p \frac{d^2 v_{C_p}}{dt^2} + (R_s + R_c) C_p \frac{dv_{C_p}}{dt} + v_{C_p} = A_i \sin(\omega t). \tag{36}$$

The output voltage is $v_s(t) = v_{C_p}(t) + v_{R_c}(t)$. At resonance, where $\omega = \omega_0$, the circuit gain with a series resistance is

$$|G_3(\omega)|_{\omega=\omega_0} = \frac{\sqrt{1+(\omega_0 R_c C_p)^2}}{\omega_0 C_q (R_s + R_c)}. \tag{37}$$

TABLE IX: Sensing circuit parameters for settling-time of 50 µs at resonance frequencies of 8 kHz and 110 kHz for the typical capsule tracking system, the parameters of which system are shown in Table II.

External resistance in	f_0 (kHz)	C_q	R_c or R_p	Gain	Gain ratio	Settling time ratio
Parallel	8	1.37 µF	8.34	0.25	0.36	0.45
	110	7.3 nF	1588	4.4	0.45	0.45
Series	8	1.37 µF	24.93	0.64	0.9	0.45
	110	7.3 nF	24.93	4.4	0.45	0.45

When $(\omega_0 R_c C_p)^2 \gg 1$, i.e., $R_c \gg \omega_0 L_s$ and $C_q \approx C_p$, the sensing circuit gain reduces to $K_s/(K_s+1)$. The settling-time variation factor $\chi_{s,ser}$ is

$$\chi_{s,ser} = \frac{1}{1+\frac{R_c}{R_s}}. \tag{38}$$

By neglecting C_s, the quality factor of the circuit is

$$Q_3 = \frac{\omega_o L_s}{(R_s+R_c)}, \tag{39}$$

which shows that the gain is proportional to resonance frequency.

C. Comparison of the Parallel and Series resistance

The variation of gain ratio and settling-time due to an external parallel and series resistance are plotted in Fig. 10. In Fig. 10 (a), it is observed that both the gain ratio and settling-time are proportional to the parallel resistance at any resonance frequency. The circuit gain is $2\pi\chi_{s,par}L_s f_0/R_s$. In Fig. 10 (b), the settling-time is inversely proportional to resistance but the gain ratio approaches an asymptote. The gain is

$$\sqrt{\left(\frac{2\pi f_0 L_s \chi_{s,ser}}{R_s}\right)^2 + (1-\chi_{s,ser})^2} \tag{40}$$

With a high resonance frequency, either the series or parallel resistance can be used since both the gain and settling-time ratios fall at the same rate. However, with a low resonance frequency, the external series resistance is preferable since the gain reduction is bounded. By calculating the frequency where both the series and parallel circuits have the same gain, the series circuit should be used if

$$f_0 \leq \frac{1}{2\pi L_s}\left(\frac{5\left(L_s + R_s R_p C_q\right)}{R_p C_q} - R_s\right). \tag{41}$$

Expressions for the required parallel or series resistance and resulting gain are summarized in Table VIII. Example sensing circuit parameters for a settling-time of 50 µs and resonance frequencies of 8 kHz and 110 kHz are also listed in Table IX. By comparing Table VII and IX, both the parallel and series configurations provide the same gain at high resonance frequency; however, the series method provides a superior gain at low resonance frequency. Notably, the required series resistance is independent of resonance frequency which is a significant practical advantage.

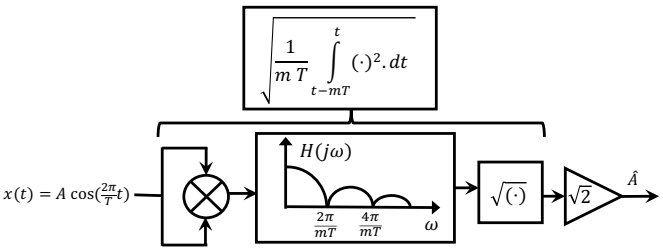

Fig. 11: Block diagram of the demodulator. $T = 1/f_0$.

IX. Measurement Rate and Bandwidth

The measurement rate and bandwidth are limited by the performance of the transmitter circuit, sensing circuit, and demodulator. The time-delay and dynamics of each system are described in the following subsections. Numerical quantities are listed for the example system described in Table II.

A. Transmitter Circuit

The settling-time of the transmitter coil current t_T is described in equation (9). Numerical values for the example system are listed in Table IV. When three coils are sequentially excited, the total settling-time is $3 \times t_T$. The settling-time of the parallel configuration is 1.45 ms, which implies a total settling-time of 4.35 ms for three coils.

B. Sensing Circuit

The settling-time and bandwidth of the sensor circuit are determined by the quality-factor of the resonance. The settling-time t_s is described in equation (31). Values for the example system are listed in Table VII. The total settling-time for nine sequentially measured voltages is $9 \times t_s$, which equates to 1 ms for the example system.

The bandwidth of the sensing circuit is described in (27). The demodulated bandwidth is

$$f_{-3\text{dB}} = \frac{1}{4\pi}\frac{R_s}{L_s} = \frac{f_0}{2Q}. \tag{42}$$

For the example system, the bandwidth is $f_{-3\text{dB}}$ = 5.66 kHz.

C. Demodulator

In this work, the moving-average RMS-to-DC demodulator is used for determining the signal amplitude [38]. This demodulator does not require a reference signal and is well suited to endoscope localization due to the low computational cost. The amplitude estimate $\widehat{A}$ is determined from

$$\widehat{A} = \sqrt{2}\sqrt{\frac{1}{mT}\int_{t-mT}^{t} x^2(t)\ dt}\ , \tag{43}$$

where T is the signal period, m is the number of periods to be averaged, and $x(t)$ is the input signal. This demodulator can be viewed as a filtering operation with a flat impulse response,

TABLE X: Measurement bandwidth and update rate with (a), and without (b), resistive tuning.

(a) With resistive tuning

System	Settling time or delay (ms)	f_{-3dB} (kHz)	Total delay (ms)	Update rate (Hz)	Maximum frequency (Hz)
Transmitter	0.30		1.57	318	318
Sensor	0.45	12.57			
Demodulator	0.82	4.84			

(b) Without resistive tuning

System	Settling time or delay (ms)	f_{-3dB} (kHz)	Total delay (ms)	Update rate (Hz)	Maximum Frequency (Hz)
Transmitter	4.35		6.17	81	81
Sensor	1.00	5.66			
Demodulator	0.82	4.84			

as illustrated in Figure 11. The transfer function of the filtering operation is

$$H(s) = \frac{1}{mTs}\left(1 - e^{-mTs}\right) \ . \tag{44}$$

The bandwidth of this system is $f_{-3dB} = 0.44/mT$. In the example system, ten periods are used for averaging, therefore, with a frequency of 110 kHz, the bandwidth is $f_{-3dB} = 4.84$ kHz.

In addition to the dynamics, the demodulator also requires a settling-time of mT to reach steady state. With nine sequential measurements, the total settling-time is $9mT$, which equates to 0.818 ms.

D. Overall Response

The maximum update rate is dictated by the total settling-time of the system t, that is

$$t = 3t_T + 9t_s + 9mT. \tag{45}$$

Assuming ideal reconstruction, the maximum frequency that can be measured has a period of $t/2$.

The bandwidth and update-rate, with and without resistive tuning, is summarized in Table X. It can be observed that the filtering effects of the sensor and demodulator are negligible due to the slow update-rate imposed by the cumulative time-delays.

X. Measurement Noise

To evaluate the impact of resonance enhanced coupling on measurement error and noise, a localization experiment is performed using the method described in reference [21]. The RMS value of the induced voltage is estimated from ten cycles using equation (43). If the actual and estimated positions are (x, y, z) and $(\widehat{x}, \widehat{y}, \widehat{z})$, the position error e is

$$e = \sqrt{(x - \widehat{x})^2 + (y - \widehat{y})^2 + (z - \widehat{z})^2}. \tag{46}$$

Assuming the transmitting coils are centered at $(0, 0, 0)$, the distance d between the transmitter and receiver is $d = \sqrt{x^2 + y^2 + z^2}$.

The average error and standard deviation of the estimated position is plotted against the transmitter-receiver distance in Fig. 12. It can be observed that both the mean error and standard deviation are significantly improved by the use of resonance.

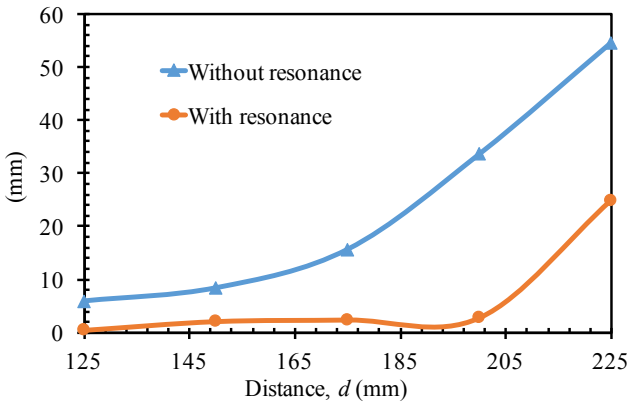

(a) Average position error

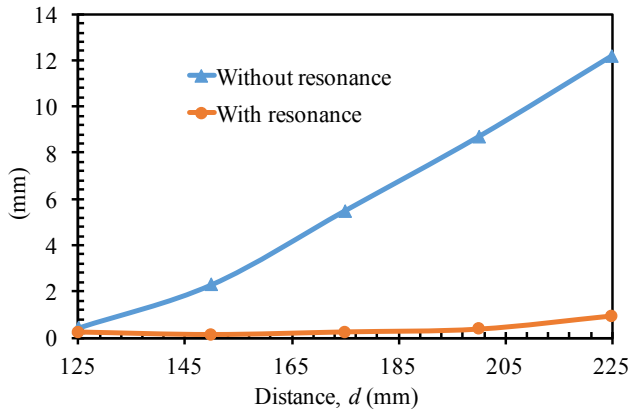

(b) Standard deviation

Fig. 12: The average position error (a) and standard deviation (b) versus the transmitter-receiver distance.

XI. Conclusion

This article investigates the application of resonance enhancement to electromagnetic tracking systems. By utilizing resonance, the transmitter efficiency can be improved, and the gain of the sensing circuit can be enhanced, both of which increase the sensing range. A resistive tuning method is proposed to optimize the trade-off between the settling-time and efficiency of the transmitter, and the settling-time and gain of the sensor.

For the transmitter, a parallel resonant circuit with an external resistance in series is preferred as long at the required source voltage is acceptable. For the sensor, a parallel resonant circuit with an external resistor in series with the capacitor is preferred.

References

[1] I. Aoki, A. Uchiyama, K. Arai, K. Ishiyama, and S. Yabukami, "Detecting system of position and posture of capsule medical device," Oct. 19 2010, uS Patent 7,815,563.

[2] S. Hashi, S. Yabukami, H. Kanetaka, K. Ishiyama, and K. Arai, "Numerical study on the improvement of detection accuracy for a wireless motion capture system," *Magnetics, IEEE Transactions on*, vol. 45, no. 6, pp. 2736–2739, 2009.

[3] S. Hashi, S. Yabukami, H. Kanetaka, K. Ishiyama, and K. I. Arai, "Wireless Magnetic Position-Sensing System Using Optimized Pickup Coils for Higher Accuracy," *IEEE Transactions on Magnetics*, vol. 47, no. 10, pp. 3542–3545, Oct. 2011.

[4] R. Graumann, "Cable-free endoscopy method and system for determining in vivo position and orientation of an endoscopy capsule," Aug. 25 2005, uS Patent App. 11/015,357.

[5] X. Guo, C. Wang, and R. Yan, "An electromagnetic localization method for medical micro-devices based on adaptive particle swarm optimization with neighborhood search," *Measurement*, vol. 44, no. 5, pp. 852–858, Jun. 2011.

[6] X.-d. Guo, G.-z. Yan, and P.-p. Jiang, "Feasibility of localizing in vivo micro-devices with electromagnetic methods," *Journal of Shanghai Jiaotong University (Science)*, vol. 13, no. 5, pp. 559–561, Nov. 2008.

[7] M. Bechtold, C. Gabriel, and A. Juloski, "Arrangement and method for navigating an endoscopic capsule," May 2 2013, uS Patent App. 13/458,937. [Online]. Available: https://www.google.com/patents/US20130109920

[8] T. Nagaoka and A. Uchiyama, "Development of a small wireless position sensor for medical capsule devices," in *Engineering in Medicine and Biology Society, 2004. IEMBS'04. 26th Annual International Conference of the IEEE*, vol. 1. IEEE, 2004, pp. 2137–2140.

[9] http://polhemus.com/.

[10] http://www.ascension-tech.com/.

[11] A. Moglia, A. Menciassi, and P. Dario, "Recent patents on wireless capsule endoscopy," *Recent Patents on Biomedical Engineering*, vol. 1, no. 1, pp. 24–33, 2008.

[12] G. Ciuti, P. Valdastri, A. Menciassi, and P. Dario, "Robotic magnetic steering and locomotion of capsule endoscope for diagnostic and surgical endoluminal procedures," *Robotica*, vol. 28, no. 02, pp. 199–207, 2010.

[13] S. Yim and M. Sitti, "Design and rolling locomotion of a magnetically actuated soft capsule endoscope," *IEEE Transactions on Robotics*, vol. 28, no. 1, pp. 183–194, 2012.

[14] X. Guo, C. Song, and R. Yan, "Optimization of multilayer cylindrical coils in a wireless localization system to track a capsule-shaped micro-device," *Measurement*, vol. 46, no. 1, pp. 117–124, jan 2013.

[15] S. Tumanski, "Induction coil sensorsa review," *Measurement Science and Technology*, vol. 18, no. 3, p. R31, 2007.

[16] M. Li, C. Hu, S. Song, H. Dai, and M. Q.-H. Meng, "Detection of weak magnetic signal for magnetic localization and orientation in capsule endoscope," in *Automation and Logistics, 2009. ICAL'09. IEEE International Conference on*. IEEE, 2009, pp. 900–905.

[17] M. R. Basar, M. Y. Ahmad, J. Cho, and F. Ibrahim, "Application of wireless power transmission systems in wireless capsule endoscopy: an overview," *Sensors*, vol. 14, no. 6, pp. 10 929–10 951, 2014.

[18] R. Carta, M. Sfakiotakis, N. Pateromichelakis, J. Thoné, D. Tsakiris, and R. Puers, "A multi-coil inductive powering system for an endoscopic capsule with vibratory actuation," *Sensors and Actuators A: Physical*, vol. 172, no. 1, pp. 253–258, 2011.

[19] R. Puers, R. Carta, and J. Thoné, "Wireless power and data transmission strategies for next-generation capsule endoscopes," *Journal of Micromechanics and Microengineering*, vol. 21, no. 5, p. 054008, 2011.

[20] B. Lenaerts and R. Puers, "An inductive power link for a wireless endoscope," *Biosensors and Bioelectronics*, vol. 22, no. 7, pp. 1390–1395, 2007.

[21] M. N. Islam and A. J. Fleming, "A novel and compatible sensing coil for a capsule in wireless capsule endoscopy for real time localization," in *IEEE SENSORS 2014 Proceedings*, Nov 2014, pp. 1607–1610.

[22] A. Plotkin and E. Paperno, "Transient-free commutation of a resonant-mode array of inductors," *Journal of Applied Physics*, vol. 97, no. 10, p. 10N507, 2005.

[23] F. H. Raab, E. B. Blood, T. O. Steiner, and H. R. Jones, "Magnetic position and orientation tracking system," *Aerospace and Electronic Systems, IEEE Transactions on*, no. 5, pp. 709–718, 1979.

[24] M. Li, S. Song, C. Hu, D. Chen, and M.-H. Meng, "A novel method of 6-dof electromagnetic navigation system for surgical robot," in *Intelligent Control and Automation (WCICA), 2010 8th World Congress on*. IEEE, 2010, pp. 2163–2167.

[25] E. Paperno, I. Sasada, and E. Leonovich, "A new method for magnetic position and orientation tracking," *Magnetics, IEEE Transactions on*, vol. 37, no. 4, pp. 1938–1940, 2001.

[26] S. Song, C. Hu, B. Li, X. Li, and M.-H. Meng, "An electromagnetic localization and orientation method based on rotating magnetic dipole," *Magnetics, IEEE Transactions on*, vol. 49, no. 3, pp. 1274–1277, 2013.

[27] J. Tian, S. Song, X. Wang, T. Yan, C. Hu, and M.-H. Meng, "An improved method and algorithm for electromagnetic localization," in *Information and Automation (ICIA), 2011 IEEE International Conference on*. IEEE, 2011, pp. 406–411.

[28] S. Song, W. Qiao, B. Li, C. Hu, H. Ren, and M. Q.-H. Meng, "An efficient magnetic tracking method using uniaxial sensing coil," *IEEE Transactions on Magnetics*, vol. 50, no. 1, pp. 1–7, 2014.

[29] S. Song, H. Ren, and H. Yu, "An improved magnetic tracking method using rotating uniaxial coil with sparse points and closed form analytic solution," *IEEE Sensors Journal*, vol. 14, no. 10, pp. 3585–3592, 2014.

[30] W. Ashe, "System and method for magnetic position tracking," Jan. 2 2014, uS Patent App. 13/534,666. [Online]. Available: http://www.google.com/patents/US20140002063

[31] W. Wang, C. Hu, W. Lin, and J. Bao, "An improved pso-based algorithm for extracting week coupling ac signal in electromagnetic localization system," in *Automation and Logistics (ICAL), 2012 IEEE International Conference on*. IEEE, 2012, pp. 623–627.

[32] J. Kuipers, "Tracking and determining orientation of object using coordinate transformation means, system and process," Sep. 28 1976, uS Patent 3,983,474. [Online]. Available: http://www.google.com.au/patents/US3983474

[33] A. Govari, "Electromagnetic position single axis system," Nov. 19 2002, uS Patent 6,484,118.

[34] Y. Zhigang and Y. Kui, "An improved 6dof electromagnetic tracking algorithm with anisotropic system parameters," in *Technologies for E-Learning and Digital Entertainment*. Springer, 2006, pp. 1141–1150.

[35] http://sixense.com/.

[36] B. Lenaerts and R. Puers, *Omnidirectional inductive powering for biomedical implants*. Springer, 2009.

[37] M. N. Islam and A. J. Fleming, "An algorithm for transmitter optimization in electromagnetic tracking systems," *IEEE Transactions on Magnetics*, vol. 53, no. 8, pp. 1–8, Aug 2017.

[38] M. G. Ruppert, D. M. Harcombe, M. R. Ragazzon, S. R. Moheimani, and A. J. Fleming, "A review of demodulation techniques for amplitude-modulation atomic force microscopy," *Beilstein Journal of Nanotechnology*, vol. 8, no. 1, pp. 1407–1426, 2017.

Mohd Noor Islam received his B.Sc in Electrical & Electronic Engineering from Khulna University of Engineering and Technology, Khulna, Bangladesh in 2003. He has completed his M.Sc in Electronic Engineering from Kookmin University, Seoul, Korea in 2009. He has been teaching as a Lecturer and then as an Assistant Professor in the Department of Electrical and Electronic Engineering in Khulna University of Engineering and Technology since 2004. Now he is pursuing his PhD in Electrical Engineering in the school of Electrical Engineering and Computer Science in the University of Newcastle, Australia. His research interests are implanted devices, robotic endoscope capsule, electromagnetic localization etc.

Dr. Andrew Fleming graduated from The University of Newcastle, Australia with a Bachelor of Electrical Engineering in 2000 and Ph.D in 2004. Dr. Fleming is now an Australian Research Council Future Fellow and Director of the Precision Mechatronics Lab at The University of Newcastle, Australia. His research includes nanofabrication, micro-robotics, meteorological sensing, nano-positioning, and high-speed scanning probe microscopy. Dr. Flemings research awards include the IEEE Transactions on Control Systems Technology Outstanding Paper Award, The University of Newcastle Researcher of the Year Award, and the Faculty of Engineering and Built Environment Award for Research Excellence. He is the co-author of three books and more than one-hundred Journal and Conference papers. Dr. Fleming is the inventor of several patent applications and in 2012 he received the Newcastle Innovation Rising Star Award for Excellence in Industrial Engagement.